INT. J. NUM. METH. HEAT FLUID FLOW, VOL. 6 NO. 2, 25–35 (1996)

THREE-DIMENSIONAL SIMULATION OF THERMALS USING A SPLIT-OPERATOR SCHEME

C. W. LI AND F. ZHANG

Department of Civil & Structural Engineering, The Hong Kong Polytechnic University, Hong Kong

ABSTRACT

A three-dimensional numerical model is developed to study the motion and mixing process induced by thermals. The model utilizes a split-operator approach for the solution of the hydrodynamic equations and the advective diffusion equation. A conservative characteristics based scheme with flux-limiter is employed to accurately approximate the advective terms in all equations and to prevent the generation of over and under shoots in the solution. In modelling the turbulent stresses and diffusion, the mixing length model is used. Cases of point thermals in uniform or stratified ambient fluid and advected line thermals are simulated and the results verify the empirical equations for thermal parameters obtained from the reported experimental data.

KEY WORDS Mixing processes Thermals Split-operator Turbulence Advection

INTRODUCTION

Thermals refer to the convective flows originated from the heating of a fluid mass or the quick release of a fluid inside another one of different density. If the density of the fluid is smaller than that of the ambient we have 'light thermals', examples include cumulus clouds and explosions. Vice-versa, we have 'dense thermals' which, for example, includes ocean dumping of sludge.

For thermals in aribtrary ambient flow and density condition, the interaction of the heavier (or lighter) fluid with the ambient fluid causes the coupling of the hydrodynamic equations and the advective-diffusion equation for fluid density. Thus, a numerical model is required to determine the flow and density variation. In addition, although experimental investigation of both point and line thermals have been reported (e.g., Wong & Lee[1], Tsang[2] and Sullivan[3]), results on the mixing characteristics for line thermals are far from conclusive. The wide scatter in the experimental constants for width and trajectory may be related to the difficulty in controlling the source condition. The use of a numerical modelling technique in this problem has the advantage that the source condition can be well controlled.

This work describes the development of a fully three-dimensional model for the study of thermal motion. A split-operator scheme is used in the solution of the governing equations. A conservative characteristics-based scheme with flux-limiter (Li & Yu[4]) is utilized to accurately predict the advective terms in all the equations. In modelling the turbulent stresses and diffusion, the mixing length model is used. Both cases of point thermals in uniform or stratified ambient fluid and advected line thermal in uniform ambient fluid are simulated. The computed results are compared with the reported experimental data.

0961–5539/96/020025–11$2.00

Received August 1994
Revised May 1995

MODEL FORMULATION

The time-averaged governing equations for thermal motion are the conservation laws of mass and momentum,

$$\frac{\partial U_l}{\partial x_l}=0 \tag{1}$$

$$\frac{\partial U_l}{\partial t}+\frac{\partial (U_l U_m)}{\partial x_m}=-\frac{1}{\rho}\frac{\partial P}{\partial x_l}+\frac{\partial}{\partial x_m}\left(\nu\frac{\partial U_l}{\partial x_m}-\overline{u_l u_m}\right)+g_l\frac{\Delta\rho}{\rho} \tag{2}$$

where $l, m=1, 2, 3$, U_l is the time-averaged velocity component in the direction x_l, P is the time-averaged static pressure minus the hydrostatic pressure, ρ is the time-averaged density of water, ν is the molecular (kinematic) viscosity, g_l is the specific body force in the direction x_l, $\Delta\rho$ is the density deficit. The Boussinesq approximation is used so that the influence of variable density appears only in the buoyancy term (the last term on the right hand side of equation (2)). $\overline{u_l u_m}$, $\overline{u_l \rho'}$ = correlations between fluctuating velocities u_l, u_m and fluctuating density ρ' due to time averaging. When multiplying by ρ, these terms represent physically the turbulence transport of momentum or mass flux, and hence are called turbulent stresses and turbulent mass flux, respectively.

The density of the fluid is influenced by the temperature (T) and/or salinity (S) and hence is variable. The relation can be approximated by,

$$\rho(S, T)=\rho(S_0, T_0)+\left.\frac{\partial\rho}{\partial T}\right|_{(S_0,T_0)}(T-T_0)+\left.\frac{\partial\rho}{\partial S}\right|_{(S_0,T_0)}(S-S_0) \tag{3}$$

and for small changes in density, we have,

$$\Delta\rho=k_1\Delta T+k_2\Delta S \tag{4}$$

where $\Delta\rho=\rho(S, T)$, $\Delta T=T-T_0$, $\Delta S=S-S_0$ and k_1, k_2 are constants. The conservation equation for the transport and diffusion of temperature excess (thermal energy) can be written as,

$$\frac{\partial\Delta T}{\partial t}+\frac{\partial(U_l\Delta T)}{\partial x_l}=\frac{\partial}{\partial x_l}(-\overline{u_l\Delta T'}) \tag{5}$$

where $\overline{u_l\Delta T'}$ is the correlation between fluctuating velocities u_l and fluctuating temperature excess $\Delta T'$ due to time averaging. In the above equation, the molecular diffusion term is neglected since it is small as compared with the turbulent diffusion term on the right hand side of the equation. Similarly, the transport and diffusion of salinity excess can be described by,

$$\frac{\partial\Delta S}{\partial t}+\frac{\partial(U_l\Delta S)}{\partial x_l}=\frac{\partial}{\partial x_l}(-\overline{u_l\Delta S'}) \tag{6}$$

The two equations can then be combined to give,

$$\frac{\partial\Delta\rho}{\partial t}+\frac{\partial(U_l\Delta\rho)}{\partial x_l}=\frac{\partial}{\partial x_l}(-\overline{u_l\Delta\rho'}) \tag{7}$$

The eddy viscosity concept is used to model the turbulent stresses,

$$-\overline{u_l u_m}=\mu\left(\frac{\partial U_l}{\partial x_m}+\frac{\partial U_m}{\partial x_l}\right) \tag{8}$$

where μ is the eddy viscosity. To specify the spatial and temporal distribution of the eddy viscosity, the mixing length model is used. The expression of μ is given by,

$$\mu=l^2\left[\left(\frac{\partial U_l}{\partial x_m}+\frac{\partial U_m}{\partial x_l}\right)\frac{\partial U_l}{\partial x_m}\right]^{1/2} \tag{9}$$

where $l=0.09$ times the nominal width of the thermal. The turbulent mass flux is generally assumed to be related to the gradient of the time average density excess,

$$-\overline{u_l \Delta\rho'}=\frac{\mu}{\sigma}\frac{\partial \Delta\rho}{\partial x_l} \tag{10}$$

where σ is the Schmidt number which is close to 1.

The boundary conditions considered are rigid free-slip walls, free water surface, inflow and outflow boundaries and a plane of symmetry. At a free water surface, $\partial U_1 \partial x_3=0$, $\partial U_2/\partial x_3=0$, $U_3=0$ (rigid-lid assumption). At an inflow boundary, $U_n=U_a$, $\partial U_{s1}/\partial n=0$, $\partial U_{s2}/\partial n=0$ and $\partial \Delta\rho/\partial n=0$, where n and $s1$, $s2$ denote the normal and tangential directions to the boundary respectively; U_a is the specified inflow velocity. At an artifically truncated boundary or an outflow boundary, $\partial U_n/\partial n=0$, $\partial U_{s1}/\partial n=0$, $\partial U_{s2}/\partial n=0$, and $\partial \Delta\rho/\partial n=0$. At a slip wall boundary or a plane of symmetry, $U_n=0$, $\partial U_{s1}/\partial n=0$, $\partial U_{s2}/\partial n=0$ and $\partial \Delta\rho/\partial n=0$.

NUMERICAL SCHEMES

The split-operator approach is used in the solution (e.g. Yanenko[5] and Benqué *et al.*[6]). The advantage of this approach is that different terms accounting for different physical processes can be treated separately by suitable schemes. At each time step, the following three solution steps are carried out,

a) Advection

$$\frac{U_l^{n+1/3}-U_l^n}{\Delta t}+\frac{\partial(U_m^n U_l^n)}{\partial x_m}=0 \tag{11}$$

$$\frac{\Delta\rho^{n+1/2}-\Delta\rho^n}{\Delta t}+\frac{\partial(U_m^n \Delta\rho^n)}{\partial x_m}=0 \tag{12}$$

b) Dispersion

$$\frac{U_l^{n+2/3}-U_l^{n+1/3}}{\Delta t}=\frac{\partial}{\partial x_m}\left(\nu\frac{\partial U_l^{n+1/3}}{\partial x_m}+\mu\left(\frac{\partial U_l^{n+1/3}}{\partial x_m}+\frac{\partial U_m^{n+1/3}}{\partial x_l}\right)\right)+g_l\frac{\Delta\rho^{n+1}}{\rho^n} \tag{13}$$

$$\frac{\Delta\rho^{n+1}-\Delta\rho^{n+1/2}}{\Delta t}=\frac{\partial}{\partial x_l}\left(\frac{\mu}{\sigma}\frac{\partial \Delta\rho^{n+1/2}}{\partial x_l}\right) \tag{14}$$

c) Pressure

$$\frac{\partial U_l^{n+1}}{\partial x_l}=0 \tag{15}$$

$$\frac{U_l^{n+1}-U_l^{n+2/3}}{\Delta t}=-\frac{1}{\rho}\frac{\partial P^{n+1}}{\partial x_l} \tag{16}$$

Advection step

At the initial stage when the heavier (or lighter) fluid acts as a point source or a line source, the induced density gradient is large and the problem is advection dominated. Significant errors will occur when usual finite difference schemes are used in the simulation of the advection terms. These include phase error, mass conservation error and over and undershoots of the solution. The presence of a negative density deficit may cause numerical instability in the coupled hydrodynamic equations. To alleviate this problem, a characteristics based scheme with a flux

limiter is adopted. The advection equation, (12), is split into three one-dimensional equations,

$$\frac{\Delta\rho^{n+1/6}-\Delta\rho^{n}}{\Delta t}+\frac{\partial(U_1^n\,\Delta\rho^n)}{\partial x_1}=0 \tag{17}$$

$$\frac{\Delta\rho^{n+1/3}-\Delta\rho^{n+1/6}}{\Delta t}+\frac{\partial(U_2^n\,\Delta\rho^{n+1/6}}{\partial x_s}=0 \tag{18}$$

$$\frac{\Delta\rho^{n+1/2}-\Delta\rho^{n+1/3}}{\Delta t}+\frac{\partial(U_3^n\,\Delta\rho^{n+1/3})}{\partial x_3}=0 \tag{19}$$

The discretization of equation (17) is given by the conservative 6-node minimax characteristics scheme (6N-MC, Li & Yu[4]),

$$\Delta\rho_i^{n+1/6}=\frac{\Delta t}{\Delta x}[(U_1\,\Delta\rho)_{i+1/2}^n-(U_1\,\Delta\rho)_{i-1/2}^n]+\Delta\rho_i^n \tag{20}$$

where

$$\begin{aligned}48(\Delta t/\Delta x)(U_1\,\Delta\rho)_{i+1/2}=&(2v-v^2-2v^3+v^4)\Delta\rho_{i-2}+(-12v+2v^2+12v^3-2v^4)\Delta\rho_{i-1}\\&+(40v+24v^3-16v^3)\Delta\rho_i-(20v-26v^2+4v^3+2v^4)\Delta\rho_{i+1}\\&+(-2v+v^2+2v^3-v^4)\Delta\rho_{i+2}\end{aligned}$$

and $v=(U_1)_i^n\,\Delta t/\Delta x$. An expression for $\Delta t/\Delta x(U_1\,\Delta\rho)_{i-1/2}$ can be derived from the above equation by proper shifting of the index. Similar expressions can be obtained for (18) and (19). The 6-node minimax-characteristics scheme utilizes interpolation from 6 grid points and takes into account the direction of advection by tracing the characteristic lines. So, 'false diffusion' arising from dispersive error is small. To avoid the generation of over and undershoots of the numerical solution a flux limiter is imposed

(i) $\Delta\rho_{i-1}^n<\Delta\rho_i^n<\Delta\rho_{i+1}^n$ or vice versa,

If $\Delta\rho_{i+1/2}^n=\max(\Delta\rho_i,\ \Delta\rho_{i+1/2},\ \Delta\rho_{i+1})$, set $\Delta\rho_{i+1/2}=\max(\Delta\rho_i,\ \Delta\rho_{i+1})$
if $\Delta\rho_{i+1/2}^n=\min(\Delta\rho_i,\ \Delta\rho_{i+1/2},\ \Delta\rho_{i+1})$, set $\Delta\rho_{i+1/2}=\min(\Delta\rho_i,\ \Delta\rho_{i+1})$
if $\Delta\rho_{i+1/2}^n=\max(\Delta\rho_i,\ \Delta\rho_{i+1/2},\ \Delta\rho_*)$, set $\Delta\rho_{i+1/2}=\max(\Delta\rho_i,\ \Delta\rho_*)$
if $\Delta\rho_{i+1/2}^n=\min(\Delta\rho_i,\ \Delta\rho_{i+1/2},\ \Delta\rho_*)$, set $\Delta\rho_{i+1/2}=\min(\Delta\rho_i,\ \Delta\rho_*)$

where $\Delta\rho_*=\Delta\rho_{i-1}+(\Delta\rho_i-\Delta\rho_{i-1})/v$

(ii) otherwise,

set $\Delta\rho_{i+1/2}=\Delta\rho_i$

Also, a discriminator is added to switch off the flux limiter around physical peaks to avoid clipping effect. Details of the discriminator can be found in Li & Yu[4]. An example on the advection of a square profile as initial condition under constant velocity is used to illustrate the performance of the scheme, The velocity is 0.5 cm/s, the grid size is 1 cm, the time step is 1 s and the travel distance of the profiles is 50 cm. From *Figure 1*, over and under shoots of the solution is apparent for the commonly used Lax-Wendroff scheme (3N-LW) and characteristics scheme using Hermitian Cubic interpolations (2N-Hc, Holly & Preissmann[7]), while the present scheme can prevent such a problem.

In the advection step, only the inflow boundary condition needed to be specified, e.g., $\Delta\rho_1^{n+1}=\Delta\rho_2^{n+1}$ for $\partial\Delta\rho/\partial x_1=0$ at $i=1$. However, the use of 6N-MC requires the estimation of density excess outside the computational domain at a known time level. The estimation is given by polynomial extrapolation, for example, $\Delta\rho_0^n=4\Delta\rho_1^n-6\Delta\rho_2^n+4\Delta\rho_3^n-\Delta\rho_4^n$, $\Delta\rho_{-1}^n=10\Delta\rho_1^n-20\Delta\rho_2^n+15\Delta\rho_3^n-4\Delta\rho_4^n$, in which the boundary node number is 1.

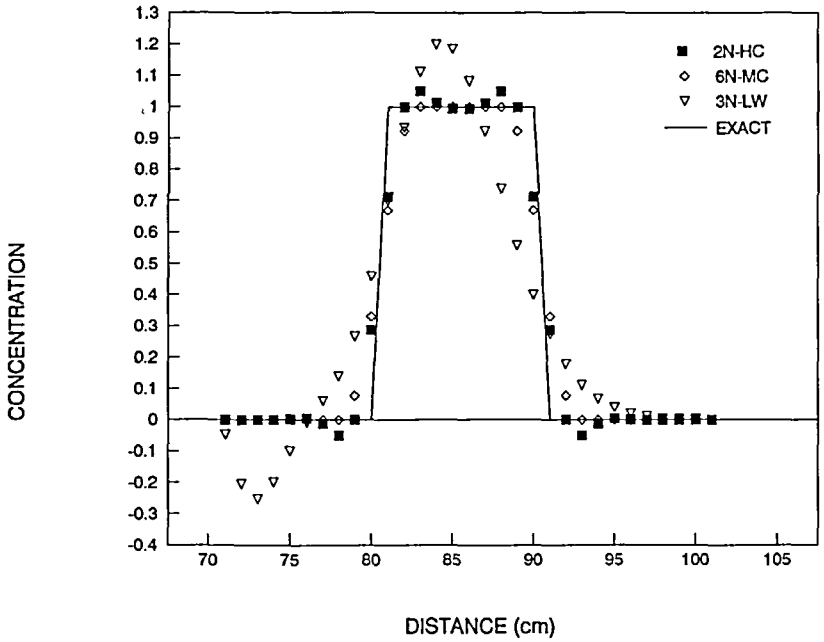

Figure 1 Pure advection of square profile under constant velocity

Diffusion step

The use of central difference scheme for equation (14) leads to,

$$\Delta\rho_{i,j,k}^{n+1}=\Delta\rho_{i,j,k}^{n+1/2}+\frac{\Delta t}{\Delta x^2}(\mu'_{i+1/2,j,k}(\Delta\rho_{i+1,j,k}^{n+1/2}-\Delta\rho_{i,j,k}^{n+1/2})-\mu'_{i-1/2,j,k}(\Delta\rho_{i,j,k}^{n+1/2}-\Delta\rho_{i-1,j,k}^{n+1/2}))$$
$$+\frac{\Delta t}{\Delta y^2}(\mu'_{i,j+1/2,k}(\Delta\rho_{i,j+1,k}^{n+1/2}-\Delta\rho_{i,j,k}^{n+1/2})-\mu'_{i,j-1/2,k}(\Delta\rho_{i,j,k}^{n+1/2}-\Delta\rho_{i,j-1,k}^{n+1/2}))$$
$$+\frac{\Delta t}{\Delta z^2}(\mu'_{i,j,k+1/2}(\Delta\rho_{i,j,k+1}^{n+1/2}-\Delta\rho_{i,j,k}^{n+1/2})-\mu'_{i,j,k-1/2}(\Delta\rho_{i,j,k}^{n+1/2}-\Delta\rho_{i,j,k-1}^{n+1/2})) \quad (21)$$

where $\mu'=\mu/\sigma$, $x=x_1$, $y=x_2$, $z=x_3$. A similar expression can be obtained for equation (13). The appropriate boundary condition can be easily incorporated into the numerical scheme, e.g. $\Delta\rho_{1,j,k}^{n+1}=\Delta\rho_{2,j,k}^{n+1}$ for $\partial\Delta\rho/\partial x_1=0$ at $i=1$.

Pressure step

By differentiating equation (16) with respect to x_l and substituting the results into equation (15), the following Poisson equation can be obtained,

$$\frac{1}{\rho}\nabla^2 P^{n+1}=\frac{1}{\Delta t}\frac{\partial U_l^{n+2/3}}{\partial x_l} \quad (22)$$

The above equation is discretized using central difference and the resulting system of equations is solved by an iterative method using successive over relaxation. The resulting finite difference

equation is given by,

$$\frac{\Delta t}{\Delta x^2}\left(\frac{P^{n+1}_{i+1,j,k}-P^{n+1}_{i,j,k}}{0.5(\rho^{n+1}_{i+1,j,k}+\rho^{n+1}_{i,j,k})}-\frac{P^{n+1}_{i,j,k}-P^{n+1}_{i-1,j,k}}{0.5(\rho^{n+1}_{i,j,k}+\rho^{n+1}_{i-1,j,k})}\right)+\frac{\Delta t}{\Delta y^2}\left(\frac{P^{n+1}_{i,j+1,k}-P^{n+1}_{i,j,k}}{0.5(\rho^{n+1}_{i,j+1,k}+\rho^{n+1}_{i,j,k})}-\frac{P^{n+1}_{i,j,k}-P^{n+1}_{i,j-1,k}}{0.5(\rho^{n+1}_{i,j,k}+\rho^{n+1}_{i,j-1,k})}\right)$$
$$+\frac{\Delta t}{\Delta z^2}\left(\frac{P^{n+1}_{i,j,k+1}-P^{n+1}_{i,j,k}}{0.5(\rho^{n+1}_{i,j,k+1}+\rho^{n+1}_{i,j,k})}-\frac{P^{n+1}_{i,j,k}-P^{n+1}_{i,j,k-1}}{0.5(\rho^{n+1}_{i,j,k}+\rho^{n+1}_{i,j,k-1})}\right)$$
$$=-\left(\frac{(U_1)^{n+2/3}_{i+1,j,k}-(U_1)^{n+2/3}_{i-1,j,k}}{2\Delta x}+\frac{(U_2)^{n+2/3}_{i,j+1,k}-(U_2)^{n+2/3}_{i,j-1,k}}{2\Delta y}\frac{(U_3)^{n+2/3}_{i,j,k+1}-(U_3)^{n+2/3}_{i,j,k-1}}{2\Delta z}\right) \quad (23)$$

Boundary conditions are required to solve the above finite difference equations. By neglecting the effect of turbulence and molecular diffusivity at a boundary, the boundary condition for the pressure can be derived from the boundary conditions for the velocities and is given by $\partial P/\partial n=0$, i.e. $P_{1,j,k}=P_{2,j,k}$ for $\partial P/\partial x_1=0$ at $i=1$. This boundary condition is valid since molecular diffusivity is small and turbulence is negligible if the boundary is far from the source of thermals.

NUMERICAL EXPERIMENTS

The first numerical experiment on thermal motion is the dumping of a heavier fluid into a stagnant uniform ambient water of density 1 g/cm^3. The volume of the heavier fluid is 0.6 cm^3 and the initial density is 1.02. The symmetrical property of the induced flow is utilized to reduce, substantially, the computational time required. A $15\times15\times35$ grid is used with $\Delta x=\Delta y=0.8$ cm and $\Delta z=1$ cm. The time step is 0.5 s. The computational domain is $0\leqslant x\leqslant15$ cm, $0\leqslant y\leqslant15$ cm, $0\geqslant z\geqslant-35$ cm. The heavier fluid is introduced at (0, 0, −3 cm) to eliminate the numerical

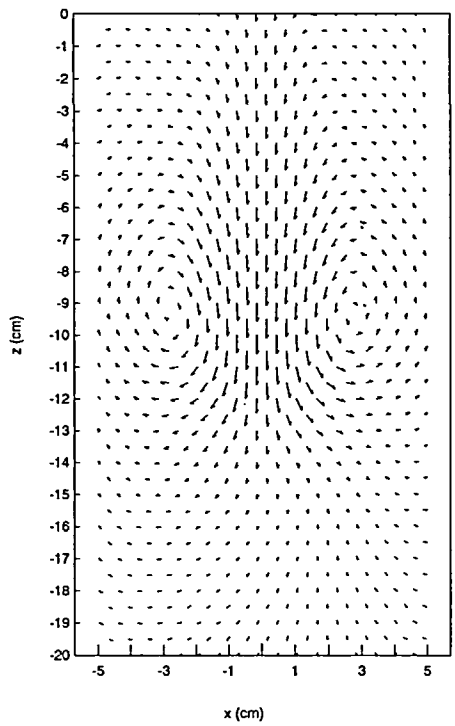

Figure 2 Velocity field at a section passing through the thermal centre at time 10 secs, maximum velocity = 1.3 cm/s

difficulty which may be otherwise generated at the free water surface. The boundary conditions are: $x=0$, plane of symmetry; $x=15$ cm, outflow boundary; $y=0$, plane of symmetry; $y=15$ cm, outflow boundary; $z=0$, rigid-lid free surface; $z=-35$ cm, outflow boundary. The simulation lasts for 20 secs and is carried out on a Pentium-90 PC. The computational time required is approximately 7 mins. In the simulation the density difference between the heavier fluid and water produces a negative buoyancy force which generates a double vortex motion. *Figure 2* depicts the double vortex structure of the flow at a section passing through the centre of the cloud at time 3 secs (only one vortex is computed and the other vortex is reproduced by symmetry). Ambient water is continuously entrained into the heavier fluid, the density excess of the cloud is reduced while the size of the cloud is increased. The linear spread of the heavier fluid is confirmed and the computed time history of the position of the centroid of the thermal,

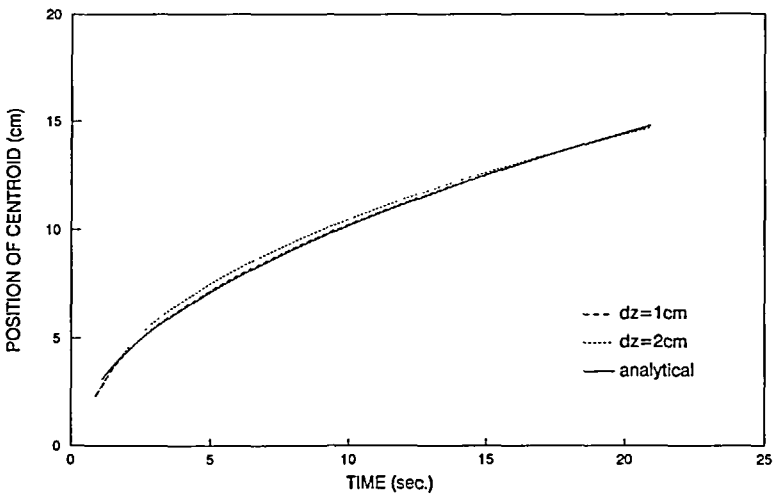

Figure 3 Variation of centroidal position with time for point thermal

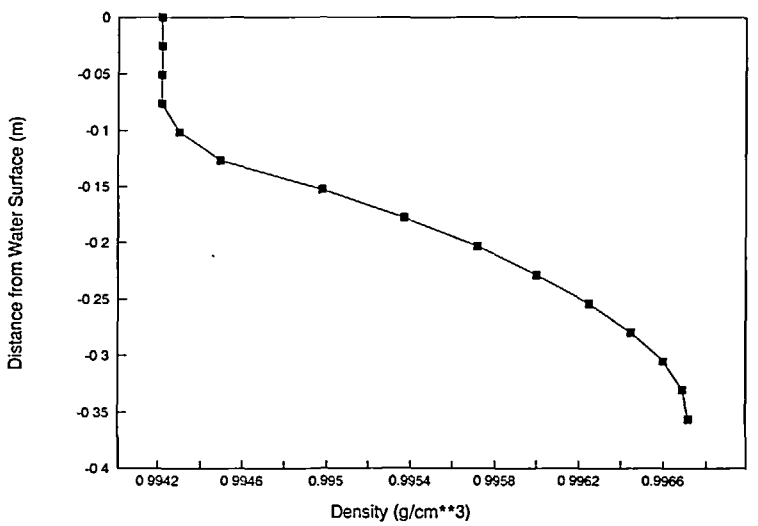

Figure 4 Density stratification of the ambient water

shown in *Figure 3*, is in good agreement with the semi-analytical relation (Sullivan[4]). The effect of grid size and the accuracy of the solution is demonstrated by repeating the computation with grid size 2 cm and time step size 0.1 s. From *Figure 3* it can be seen that the difference between the computed position of the centroid of the cloud in the two cases is small (with a maximum difference of about 5%).

The second numerical experiment is the dumping of heavier fluid into a stratified ambient. The stratification is shown in *Figure 4*. The volume of the heavier fluid is 3.66 cm^2 and the initial density is 1.0655 g/cm^3. Symmetrical property of the induced flow is considered to reduce the required computational time. A $15 \times 15 \times 35$ grid is used with $\Delta x = \Delta y = 0.8$ cm and $\Delta z = 1$ cm. The time step used is 0.025 secs. The computational domain is $0 \leqslant x \leqslant 15$ cm, $0 \leqslant y \leqslant 15$ cm, $0 \geqslant z \geqslant -35$ cm. The heavier fluid was introduced at (0, 0, −3 cm) to eliminate the numerical difficulty at the free water surface. The boundary conditions are: $x = 0$, plane of symmetry; $x = 15$ cm, outflow boundary; $y = 0$, plane of symmetry; $y = 15$ cm, outflow boundary; $z = 0$, rigid-lid free surface; $z = 35$ cm, outflow boundary. The simulation lasts for 15 secs and the computational time required is approximately 25 mins on a Pentium-90 PC. The computational time is greater than that in the first numerical experiment because more iterations are required for the convergence of the solution, at each time step, due to the presence of nonlinear ambient density profile. In the simulation the heavier fluid descends downward and entrains the ambient water with its density being decreased. At the place where the density of the heavier fluid is equal to the density of the ambient water, the heavier fluid slightly over shoots downward and then rebounds and finally comes to rest. *Figure 5* depicts the trajectory of the thermal, which is in satisfactory agreement with the experimental results (Koh & Chang[8]). *Figure 6* depicts the typical flow field at a cross-section passing through the centre of the thermal when the thermal stops descending, two pairs of current vortexes are clearly observed. The effect of grid size and the accuracy of the solution are demonstrated by repeating the computation with grid size 2 cm and time step size 0.05 s, as well as with grid size 0.5 cm and time step size 0.5 s. From *Figure 5* it can be seen that the difference in the computed position of the centroid of the cloud among all the simulations is small (with a maximum difference less than 5%). It is interesting to note that the convergence of the solution is not monotonic, probably because of the nonlinear ambient density profile.

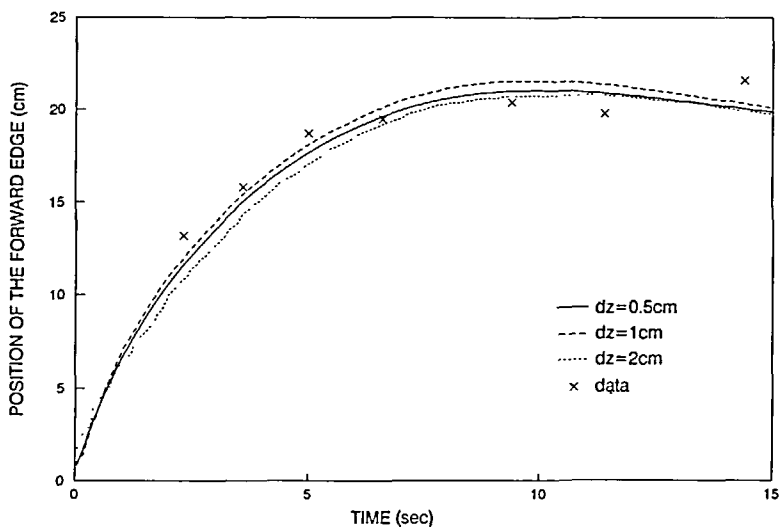

Figure 5 Position of forward edge (cm) of the thermal with time

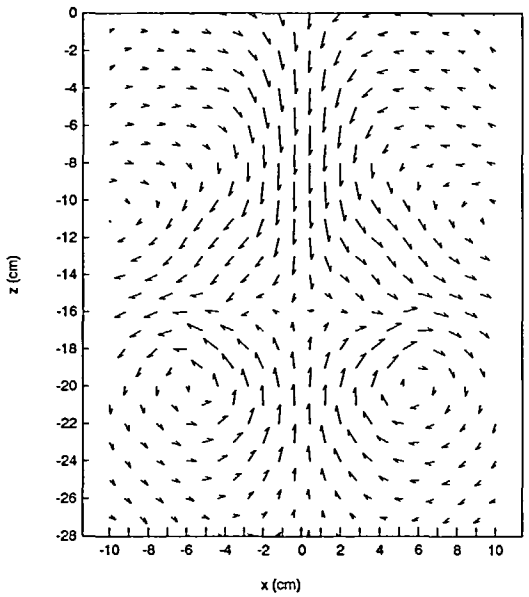

Figure 6 Velocity field at a section passing through the thermal centre at time 15 sec, maximum velocity = 0.73 cm/s.

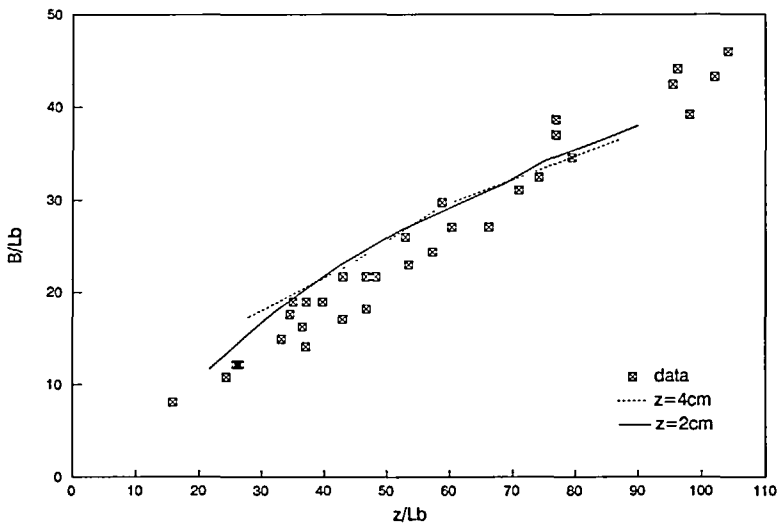

Figure 7 Nominal width of the advected line thermal

The last numerical experiment is on advected line thermal which is generarated by continuous discharge of heated water in a submerged pipe in a co-flowing current with the same velocity U as the discharge jet. As there is no excess horizontal momentum, the buoyancy induced flow viewed in a reference frame moving at velocity U resembles a vertically rising line thermal. In the computation, $U = 5$ cm/s, $\Delta\rho_0/\rho_0 = 0.018$. The diameter of the jet D is 1 cm. A $20 \times 15 \times 45$ grid is used with $\Delta x = 20$ cm, $\Delta y = 2$ cm and $\Delta z = 2$ cm. The time step is 0.2 secs. The computational domain is $0 \leqslant x \leqslant 400$ cm, $0 \leqslant y \leqslant 30$ cm, $0 \geqslant z \geqslant -90$ cm. To avoid numerical difficulty at the boundary, the discharge point is set at (100 cm, 0 cm, -80 cm). At each time step, the exact

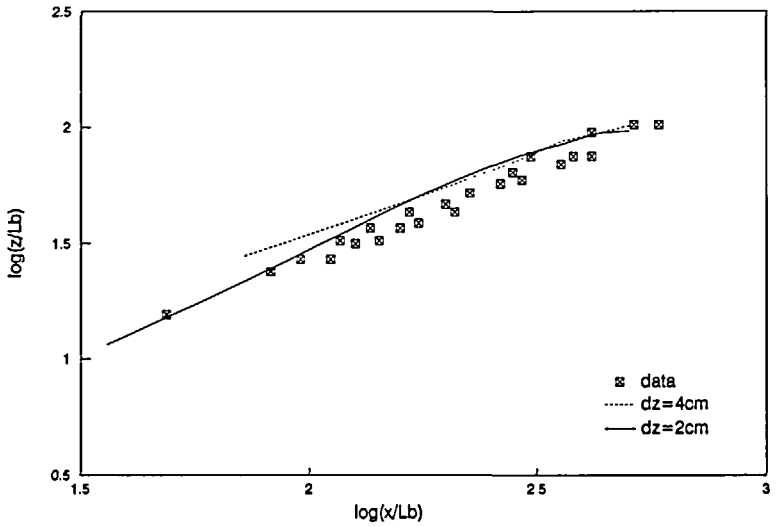

Figure 8 Trajectory of the centreline density of the advected line thermal $\left(Lb=\frac{\Delta\rho}{\rho}g\frac{\pi D^2}{4}\frac{1}{U^2}\right)$

amount of the density excess is added to the solution at the discharge point. The boundary conditions are: $x=0$, free-slip wall; $x=400$ cm, outflow boundary; $y=0$, plane of symmetry; $y=30$ cm, outflow boundary; $z=0$, rigid-lid free surface; $z=-90$ cm, outflow boundary. The simulation lasts for 80 secs and the computational time required is approximately 25 mins on a Pentium-90 PC. Steady state solution is obtained after approximately 80 secs. At steady state, the spread of the thermal width B with rising distance z is approximately linear and the computed solution is in acceptable agreement with the data reported (Wong & Lee[1]), as shown in *Figure 7*. Also the computed trajectory of the line thermal is in acceptable agreement with the data by Wong & Lee[1] (*Figure 8*). The effect of grid size and hence the accuracy of the solution is studied by repeating the computation with grid size $\Delta x=40$ cm, $\Delta y=\Delta z=4$ cm and time step size 0.4 secs. From *Figures 7–8*, it can be seen that the difference in the computed cloud width and the difference in the computed trajectory for the two cases of simulation are small at location not close to the discharge point, whereas apparent differences are observed at location close to the discharge point. Large numerical errors occur around the source because the grid is too coarse as compared to the cloud size there.

CONCLUSIONS

A three-dimensional numerical model has been developed to simulate the mixing process and motion induced by a thermal. The split-operator approach is used in the numerical algorithm to represent different physical processes by suitable numerical schemes. In particular, a conservative characteristics based scheme with flux-limiter has been used to discretize the advective terms. The numerical model has been applied to simulate point thermals in uniform or stratified ambient fluid and advected line thermal in a uniform ambient fluid. The results are in satisfactory agreement with the reported experimental data.

REFERENCES

1 Wong, C. F. and Lee, J. H. W. Experiments on advected line thermals, *Proc. Int. Symp. on Environmental Hydraulics*, Hong Kong, Dec., 153–157 (1991)
2 Tsang, G. Laboratory study of line thermals, *Atmospheric Environment*, **5**, 445–471 (1971)
3 Sullivan, P. J. The penetration of a density interface by heavy vortex rings, *Water, Air and Soil Pollution*, **1**, 322–336 (1972)
4 Li, C. W. and Yu, T. S. Conservative characteristics-based schemes for mass transport, *J. Hyd. Eng.*, ASCE, 1089–1099 (1994)
5 Yanenko, N. N. *The Method of Fractional Steps*, Springer (1971)
6 Benqué, J. P. *et al.* A new finite element method for Navier-Stokes equations coupled with a temperature equation, *Proc. 4th Int. Symp. Finite Elements in Flow Problems*, 295–302 (1982)
7 Holly, F. M. Jr. and Preissmann, A. Accurate calculation of transport in two dimensions, *J. Hydr. Div. ASCE*, **103** (HY11), 1259–1277 (1977)
8 Koh, R. C. Y. and Chang, C. *Mathematical Model for Barged Ocean Disposal of Wastes*, Report No. 660-2-73-029, U.S. Environmental Protection Agency (1973)